Available online at www.sciencedirect.com
ScienceDirect
International Journal of Heat and Fluid Flow 29 (2008) 306–314
International Journal of HEAT AND FLUID FLOW
www.elsevier.com/locate/ijhff

Soret effect on thermosolutal convection developed in a horizontal shallow porous layer salted from below and subject to cross fluxes of heat

A. Mansour, A. Amahmid *, M. Hasnaoui

University Cadi Ayyad, Faculty of Sciences Semlalia, Department of Physics, UFR TMF, BP 2390 Marrakech, Morocco

Received 7 August 2006; received in revised form 20 May 2007; accepted 4 July 2007
Available online 14 August 2007

Abstract

Combined effect of thermodiffusion and lateral heating on double diffusive natural convection in a horizontal porous layer, filled with a binary fluid and subjected to uniform fluxes of heat and mass on its long sides, is studied analytically and numerically. The short sides of the layer are impermeable to mass transfer and exposed to a perturbating constant heat flux. The governing parameters of problem under study are the Rayleigh number R_T, the Lewis number Le, the buoyancy ratio N, the separation parameter φ, the ratio of the horizontal to vertical heat flux a and the aspect ratio A_r of the layer. The thermodiffusion effect on the multiplicity of solutions is studied. It is demonstrated that the φ–N plane can be divided into four regions presenting different behaviors. The heat transfer is found to be considerably affected by the Soret effect.

Keywords: Thermosolutal convection; Porous medium; Analytical and numerical study; Multiplicity of solutions; Soret effect

1. Introduction

Thermodiffusion in binary fluids is a subject of intensive research due to its wide range of applications in many engineering and technological areas. These include geophysics, oil reservoirs, multi-component melts and storage of nuclear wastes and many other applications.

Recent experimental studies on the thermodiffusion phenomenon proved the existence of mixtures (ferrofluids, polymers, sodium chloride in compact clays, ...) for which the soret coefficient is large enough to affect considerably the flow and heat and mass transfer in these mixtures. Rosanne et al. (2003) studied experimentally the thermodiffusion in a solution of sodium chloride contained in compact clay. They concluded that the mass transfer is enhanced by the thermal diffusion. The Soret coefficient is found to be very large ($|S_T| > 5 \times 10^{-2}\,K^{-1}$) and its sign is related to the respective directions of the temperature and concentration gradients. Platten and Costesèque (2004) determined experimentally the Soret coefficient in a pure fluid and in a porous medium and concluded that this coefficient is the same for both media. Benano-Melly et al. (2001) studied numerically and experimentally the problem of thermo-diffusion in an initially homogeneous mixture submitted to a horizontal thermal gradient. Their numerical results showed that, depending on the Soret number value, multiple convection-roll flow patterns could develop in the presence of counter-acting thermal and solutal buoyancy forces. The Soret effect on convection in a horizontal porous cavity submitted to cross gradients of temperature and concentration was considered by Bennacer et al. (2003). Their results showed that, when the vertical concentration gradient is stabilizing, multiple steady-state solutions become possible over a range of buoyancy ratios which is strongly dependent on the Soret parameter. Mansour et al. (2006) studied numerically the

* Corresponding author. Tel.: +212 24 43 46 49x489; fax: +212 24 43 74 10.
E-mail address: amahmid@ucam.ac.ma (A. Amahmid).

0142-727X/$ - see front matter © 2007 Elsevier Inc. All rights reserved.
doi:10.1016/j.ijheatfluidflow.2007.07.002

Nomenclature

A_r	aspect ratio ($=L'/H'$)
D	mass diffusivity
D^*	thermo-diffusion coefficient
g	gravitational acceleration
H'	height of the porous cavity
j'	constant mass flux per unit area
K	permeability of the porous medium
L'	length of the porous cavity
Le	Lewis number ($Le = \alpha/D$)
M	parameter characterizing the Soret effect ($M = D^* S'_0 \Delta T'/D\Delta S'$)
N	buoyancy ratio ($N = \beta_S \Delta S'/\beta_T \Delta T'$)
Nu	Nusselt number
q'	constant heat flux per unit area
R_T	thermal Darcy–Rayleigh number ($R_T = g\beta_T K q' H'^2/(\lambda\alpha\nu)$)
S	dimensionless solute concentration [$S = (S' - S'_0)/\Delta S'$]
S'_0	dimensional solute concentration at the cavity centre
$\Delta S'$	concentration solute difference ($\Delta S' = j' H'/D$)
Sh	Sherwood number
T	dimensionless temperature ($T = (T' - T'_0)/\Delta T'$)
t	dimensionless time ($t = t'\alpha/\sigma H'^2$)
T'_0	dimensional temperature at the cavity centre
$\Delta T'$	temperature difference ($\Delta T' = q' H'/\lambda$)
u	dimensionless horizontal velocity ($u = u' L'/\alpha$)
v	dimensionless vertical velocity ($v = v' L'/\alpha$)
x	dimensionless distance along the x axis ($x = x'/L'$)
y	dimensionless distance along the y axis ($y = y'/L'$)

Greek symbols

α	thermal diffusivity ($\alpha = \lambda/(\rho C)_f$)
β_S	solutal expansion coefficient
β_T	thermal expansion coefficient
ε	normalized porosity ($\varepsilon = \varepsilon'/\sigma$)
ε'	porosity of the porous medium
φ	separation ratio
λ	thermal conductivity of the saturated porous medium
ν	kinematic viscosity of the fluid
π	density of the fluid mixture
$(\rho c)_f$	heat capacity of fluid mixture
$(\rho c)_p$	heat capacity of the saturated porous medium
σ	heat capacity ratio ($\sigma = (\rho c)_p/(\rho c)_f$)
Ψ	dimensionless stream function ($\Psi = \Psi'/\alpha$)

Superscript

$'$	dimensional variables

Soret effect on fluid flow and heat and mass transfer induced by double diffusive natural convection in a square porous cavity submitted to cross gradients of temperature and concentration. They concluded that the Soret effect may affect considerably the heat and mass transfer in the medium; it leads to an enhancement or to a reduction of the mass transfer, depending on the flow structure and the sign of the Soret parameter. Er-Raki et al. (2006) studied the soret effect on boundary layer flows induced in a vertical porous layer subjected to horizontal fluxes of heat and mass. It was found that, depending on the sign of the buoyancy ratio, the boundary layer thickness can increase or decrease with the Soret parameter.

Efforts have also been devoted to study the Soret effect on the onset of convection flows in rectangular enclosures. Hence, Rehberg and Ahlers (1985) studied experimentally bifurcations phenomena in a horizontal porous layer of normal-fluid 3He–4He mixture heated from below. Their study showed that the nature of bifurcation from the rest state depends on the separation ratio. Joly et al. (2001) studied analytically and numerically the onset of natural convection within a vertical porous layer subject to uniform heat fluxes along the vertical walls using the Brinkman-extended Darcy model. It is found that both supercritical and subcritical bifurcations are possible in this system. Soret effect, combined with gravity gradient, on the onset of thermosolutal convection in a fluid saturated porous layer was studied by Alex and Patil (2001). Ryskin et al. (2003) studied the Soret effect on thermo-convection in a horizontal infinite layer of binary liquid mixtures with weak concentration diffusivity and large separation numbers. Considering the study relevant to ferrofluids, they worked with a separation ratio varying in the range $[0, 100]$ (they also reported that the separation ratio may be as smaller as -200). They showed that both linear and nonlinear convective behaviors were significantly altered by the concentration field as compared to single-component systems in the case of a classical Rayleigh Bénard problem. Bourich et al. (2005) studied analytically and numerically the Soret effect on thermal natural convection within a horizontal porous enclosure uniformly heated from below by a constant heat flux using the Brinkman-extended Darcy model. It is found that the separation parameter has a strong effect on the thresholds of instabilities and on the heat and mass transfer characteristics. Other investigations devoted to study the Soret effect on the onset of convection in binary mixtures can be found in the papers by Marcoux et al. (1998), Sovran et al. (2001), Karcher and Müller (1994), Bahloul et al. (2003) and Bourich et al. (2004a).

The object of the present study is to examine the influence of the Soret effect on the natural convective flows

induced within a shallow enclosure heated and salted from below with constant heat and mass fluxes and submitted to a lateral perturbating heat flux. The results obtained show that different behaviors can be observed depending on the values attributed to the parameter characterizing the Soret effect.

2. Mathematical formulation

The system under study (sketched in Fig. 1) is a two-dimensional horizontal porous layer of width L' and height H'. The short walls of the layer are impermeable and exposed to a constant heat flux of intensity aq', while its long horizontal walls are subject to uniform fluxes of heat, q', and mass j'. The porous medium is assumed to be homogeneous and isotropic and inertia effects are neglected. The diluted binary solution that saturates the porous matrix is modeled as a Boussinesq incompressible fluid and the physical properties of the medium are assumed constant. Using the Darcy model and taking into account the Soret effect, the dimensionless governing equations are written as follows:

$$\nabla^2\Psi = -R_T\left(\frac{\partial T}{\partial x} + N\frac{\partial S}{\partial x}\right) \tag{1}$$

$$\nabla^2 T = \frac{\partial T}{\partial t} + \frac{\partial(uT)}{\partial x} + \frac{\partial(vT)}{\partial y} \tag{2}$$

$$\frac{1}{Le}(\nabla^2 S + M\nabla^2 T) = \varepsilon\frac{\partial S}{\partial t} + \frac{\partial(uS)}{\partial x} + \frac{\partial(vS)}{\partial y} \tag{3}$$

$$u = \frac{\partial\Psi}{\partial y}, \quad v = -\frac{\partial\Psi}{\partial x} \tag{4}$$

where Ψ, T and S are the dimensionless stream function, temperature and concentration, respectively.

The boundary conditions associated to the problem are such that:

$$\Psi = 0, \quad \frac{\partial T}{\partial x} = -a; \quad \frac{\partial S}{\partial x} = aM \quad \text{for } x = \pm\frac{A_r}{2} \tag{5}$$

$$\Psi = 0, \quad \frac{\partial T}{\partial y} = -1; \quad \frac{\partial S}{\partial y} = -1 + M \quad \text{for } y = \pm\frac{1}{2} \tag{6}$$

The parameter M $\left(M = \frac{D^* S_0' \Delta T'}{D \Delta S'}\right)$, appearing in the concentration equation and its associated boundary conditions characterizes the Soret effect. Its use allows the reproduction of the results obtained in the absence of Soret effect, just by setting $M = 0$. This normalization is similar to that used in the past by Alex and Patil (2001) and some other authors. However, by determining the regions leading to different types of solutions, we judge more appropriate the use of the separation ratio $\varphi = MN$ instead of M to characterize the Soret effect. Note that the value $\varphi = 0$ corresponds to the case of double diffusive convection without Soret effect and the definition of the buoyancy ratio, N, is based on the imposed mass flux j'. Thus, the case $N = 0$ corresponds to horizontal boundaries impermeable to mass transfer (i.e. $j' = 0$).

3. Numerical solution

The numerical solution of the full governing equations was obtained using a second order finite-difference scheme. The temperature and concentration equations, Eqs. (2) and (3), were solved iteratively using the alternate direction implicit method. Nodal values of the stream function were obtained, from Eq. (1), via a point successive-over-relaxation method. Details concerning the validation of the present code in the absence of Soret effect are given in the paper by Bourich et al. (2004b). In the presence of Soret effect, the numerical code was successfully used by Bourich et al. (2004a) to reproduce, with a good accuracy, the results of an analytical solution developed in the case of a horizontal porous layer subject to vertical fluxes of heat and mass. A grid size of 301×61 was found enough to recover the analytical results. As the analytical solution is valid for large aspect ratios enclosures, $A_r \geqslant 10$ was used for all the numerical calculations. A globally non uniform grid was considered in the horizontal direction to capture the flow details in the end regions of the cavity.

4. Results and discussion

4.1. Analytical solution

For the present problem, the parallel flow approximation is confirmed numerically in terms of streamlines, isotherms and iso-solutes presented in Fig. 2. It can be seen from this figure that, in the core region of the cavity, the flow is parallel to the long sides and the temperature and

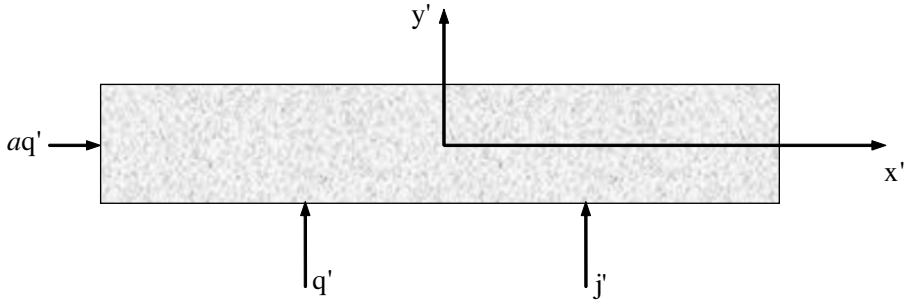

Fig. 1. Schematic of the physical system.

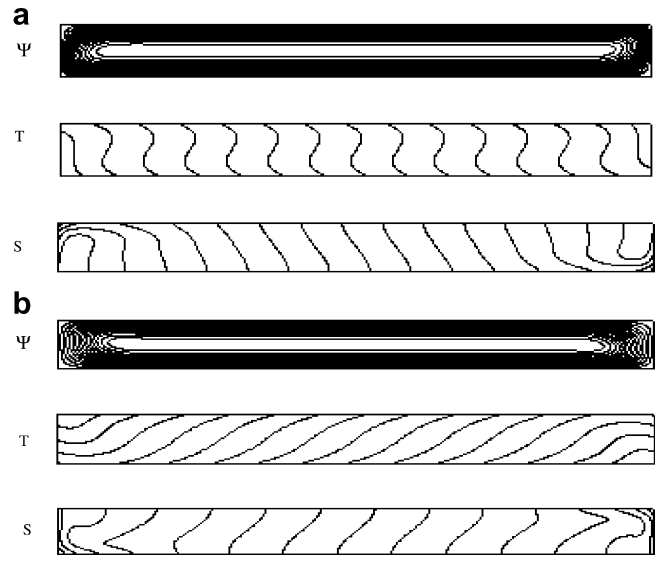

Fig. 2. Streamlines, isotherms and concentration contours for $A_r = 10$, $R_T = 50$, $Le = 10$, $N = 2$, $\varphi = 2$ and $a = 0.4$. (a) Clockwise flow ($\Psi_{min} = -3.05$, $\Psi_{max} = 0$, $Nu = 5.89$ and $Sh = 53.97$) and (b) counter-clockwise flow ($\Psi_{min} = 0$, $\Psi_{max} = 2.22$, $Nu = 1.78$ and $Sh = 54.48$).

concentration fields are characterized by a linear stratification in the horizontal direction. These observations allow the simplifications $T(x,y) = C_T x + \theta_T(y)$, $S(x,y) = C_S x + \theta_S(y)$ and $\Psi(x,y) = \Psi(y)$ and lead to the following set of ordinary equations:

$$\frac{d^2\Psi}{dy^2} = -R_T(C_T + NC_S) \tag{7}$$

$$\frac{d^2\theta_T}{dy^2} = C_T\frac{d\Psi}{dy} \tag{8}$$

$$\frac{d^2\theta_S}{dy^2} = LeC_S\frac{d\Psi}{dy} \tag{9}$$

with the associated boundary conditions in the y-direction:

$$\Psi = 0, \quad \frac{\partial\theta_T}{\partial y} = -1, \quad \frac{\partial\theta_S}{\partial y} = -1 + M \quad \text{for } y = \pm\frac{1}{2} \tag{10}$$

The determination of the constants C_T and C_S is based on heat and solute balances across any transversal section of the cavity (Trevisan and Bejan (1986)), which yields the following integrals:

$$\int_{-0.5}^{0.5}\left(uT - \frac{\partial T}{\partial x}\right)dy = a \quad \text{and}$$
$$\int_{-0.5}^{0.5}\left[uS - \frac{1}{Le}\left(\frac{\partial S}{\partial x} + M\frac{\partial T}{\partial x}\right)\right]dy = 0 \tag{11}$$

Solutions of Eqs. (7)–(9) satisfying the boundary conditions (10) are:

$$\Psi(y) = \Psi_0(1 - 4y^2) \tag{12}$$

$$T(x,y) = C_T x - y - 4\Psi_0 C_T\left(\frac{y^3}{3} - \frac{y}{4}\right) \tag{13}$$

$$S(x,y) = C_S x + (M-1)y - 4\Psi_0(LeC_S + C_T)\left(\frac{y^3}{3} - \frac{y}{4}\right) \tag{14}$$

where Ψ_0 is the value of Ψ at the centre of the porous layer given by

$$\Psi_0 = \frac{R_T}{8}(C_T + NC_S) \tag{15}$$

The heat and solute transfers in the layer are characterized by the Nusselt and Sherwood numbers as

$$Nu = \frac{1}{[T(0,-1/2) - T(0,1/2)]} = \frac{3}{3 - 2C_T\Psi_0} \tag{16}$$

$$Sh = \frac{1}{[S(0,-1/2) - S(0,1/2)]} = -\frac{3}{3(M-1) + 2\Psi_0(LeC_S - MC_T)} \tag{17}$$

where

$$C_T = \frac{-5(3a - 2\Psi_0)}{15 + 8\Psi_0^2} \quad \text{and}$$

$$C_S = \frac{-10Le\Psi_0(M-1) + MC_T(8Le\Psi_0^2 - 15)}{15 + 8Le^2\Psi_0^2} \tag{18}$$

Substituting Eq. (18) into Eq. (15) yields the following equation for Ψ_0:

$$\Psi_0^5 + A\Psi_0^3 + B\Psi_0^2 + C\Psi_0 + D = 0 \tag{19}$$

where $A = 80d[12(Le^2+1) - R_T Le(N+Le)]$, $B = 120da - R_T Le(Le+\varphi)$, $C = -150dR_T[(NLe+1) - \varphi(Le+1)] + 1800d$, $D = 225daR_T(1-\varphi)$, $d = \frac{1}{512Le^2}$ and $\varphi = MN$.

For given values of R_T, Le, N, M and a, Eq. (19) can be solved numerically.

By setting $\Psi_0 = 0$, the purely diffusive state is obtained:

$$T(x,y) = -ax - y \tag{20}$$

$$S(x,y) = aMx + (M-1)y \tag{21}$$

$$Nu = 1 \quad \text{and} \quad Sh = \frac{1}{1-M} = \frac{1}{1-\varphi/N} \tag{22}$$

Eq. (22) indicates that the concentration profile depends on the Soret effect even in the absence of fluid flow and the Sh corresponding to the purely diffusive regime is a function of φ.

To perform a quick analysis of the number of possible parallel flow solutions for this problem, we consider Eq. (19) in the case of large R_T. Solutions with Ψ_0 presenting asymptotic limits at large R_T verify:

$$\Psi_0^3 + a_1\Psi_0^2 + b_1\Psi_0 + c_1 = 0 \tag{23}$$

$$\text{where } \begin{cases} a_1 = 120daR_T Le(Le+\varphi)/A_1 \\ b_1 = -150dR_T[(NLe+1) - \varphi(Le+1)]/A_1 \\ c_1 = 225daR_T(1-\varphi)/A_1 \\ A_1 = -80dR_T Le(N+Le)]. \end{cases}$$

By introducing the variable $\Psi_1 = \Psi_0 + \frac{a_1}{3}$, Eq. (23) becomes:

$$\Psi_1^3 + p\Psi_1 + q = 0 \tag{24}$$

where $p = b_1 - \frac{a_1^2}{3}$ and $q = \frac{2}{27}a_1^3 - \frac{a_1 b_1}{3} + c$.

The discriminant of this equation is $\Delta = q^2 + \frac{4}{27}p^3$. Then Eq. (24) has one or three real solutions, depending on the sign of Δ (one solution if $\Delta > 0$ and three solutions if $\Delta < 0$). Furthermore two other solutions, with Ψ_0 increasing monotonically with R_T, may also be obtained; they satisfy $\Psi_0^2 - 80dLe(N + Le)R_T = 0$. Then, $\Psi_0 = \pm[80dLe(N + Le)R_T]^{1/2}$. These solutions are existing only for $N > -Le$ and vary as $R_T^{1/2}$. Thus, it is clear that up to five parallel flow solutions are possible in the present problem. Based on these asymptotic developments and on other numerical considerations (resolution of Eq. (19)), it is found that the φ–N plane can be divided into four regions with specific behaviors as illustrated in Fig. 3 for $a = 0.2$ and $Le = 10$. Note that, in a given region, the passage from a zone with $\varphi > 1$ to another with $\varphi < 1$ leads to the disappearance of one trigonometric solution and the latter is replaced by a clockwise one. In Fig. 3, region I is defined by $N < N_1$ (N_1 being the first root of $\Delta = 0$ for a given φ) and it is characterized by a single parallel flow solution that exists for any $R_T > 0$. In this region, only the rest state solution is existing for $\varphi = 1$. Region II, which is large in the lower part ($\varphi < -9.95$) of the figure and very thin in its upper part, is delineated by $N_1 < N < -\mathrm{Le}$. Three solutions are possible in this region; one is existing for any $R_T > 0$ and the two others appear only when R_T exceeds some critical value which depends on the other parameters. The region III, characterized by a large upper part and a very thin lower part, is delineated by $-\mathrm{Le} < N < N_2$ ($N_2 > N_1$ being the second root of $\Delta = 0$ for a given φ). The first solution, among the five solutions existing in this region, starts from $R_T = 0$. The other solutions appear by pair at two different critical values of R_T. In the last region, characterized by $N > N_2$, three solutions are possible for large R_T but, in this region, there is a small zone, adjacent to the boundary $N = N_2$, where five solutions are possible for an intermediate range of R_T. It is to recall that all the solutions of region II are such that Ψ_0 presents an asymptotic limit with R_T, while in regions III and IV, Ψ_0 varies as $R_T^{1/2}$ for two among the exiting solutions.

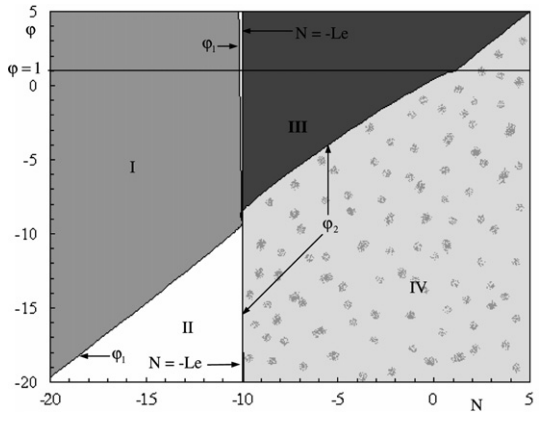

Fig. 3. Regions corresponding to different behaviors in the φ–N plane for $a = 0.2$ and $Le = 10$.

4.2. Effect of R_T for different regions

In all the figures presented in this study, the continuous lines correspond to the analytical solutions validated numerically (stable solutions) while the dashed lines represent the "unstable solutions"; those not obtained numerically. However, a perturbation method is required to obtain more precise information about the stability of the solution. Note also that the clockwise solutions are characterized by $\Psi_0 < 0$ while the trigonometric ones are characterized by $\Psi_0 > 0$.

The effect of R_T on the fluid flow and heat and mass transfer characteristics depends on the values attributed to the other governing parameters. The evolution of the flow intensity Ψ_0, the Nusselt number, Nu, and the Sherwood number, Sh, with R_T is presented in Figs. 4a–c for $Le = 10$, $a = 0.2$, $\varphi = 2$ and various N. For $N = 5$, Fig. 4a shows that only one convective stable trigonometric solution is obtained for $R_T < 0.57$. Above this threshold of R_T, two additional clockwise rotating solutions appear. The flow intensity, $|\Psi_0|$, corresponding to the stable solutions increases with R_T, while that corresponding to the unstable branches has an asymptotic evolution. For $N = 2.3$, four ranges of R_T are identified. In fact, only one solution exits in the range $0 < R_T < 5.49$. The number of solutions rises to three for $5.49 < R_T < 19.42$ and to five for $19.42 < R_T < 23.29$ and drops again to three when R_T exceeds 23.29. Note that, for $R_T > 23.29$, the evolution of the flow intensity is qualitatively similar to that corresponding to $N = 5$. For $N = 2$, a single trigonometric solution exists for $R_T < 7.58$ and, above this limit, two additional clockwise solutions appear, followed by two trigonometric ones when R_T exceeds 22.41. The flow intensity of three among the five solutions exhibits an asymptotic behavior with R_T. It should be noted that, the branch starting from $R_T = 0$ could not be obtained numerically when R_T exceeds 15; this branch becomes probably unstable above some threshold of R_T.

The evolution, with R_T, of the Nusselt number, corresponding to the different solutions described above, is presented in Fig. 4b. Generally, Nu induced by the trigonometric stable branches undergoes a very slight decrease with R_T, limited to small values of R_T and not visible on the curves. This behavior is attributed to the lateral flux which heats the fluid coming from the cold wall. The decrease in the evolution of Nu is followed by a fast increase with R_T while Nu induced by the unstable branches decreases with R_T towards an asymptotic limit. Comparatively, the best heat transfer is induced by a clockwise stable solution for a given set of the governing parameters.

The evolution of Sh with R_T, presented in Fig. 4c, shows complex and interesting behaviors for the different solutions. Hence, for $N = 5$, both stable solutions induce nearly the same Sh which increases slowly towards an asymptotic limit as R_T is increased, while the unstable solution induces nearly a constant Sh ($Sh \approx 0.657$). For

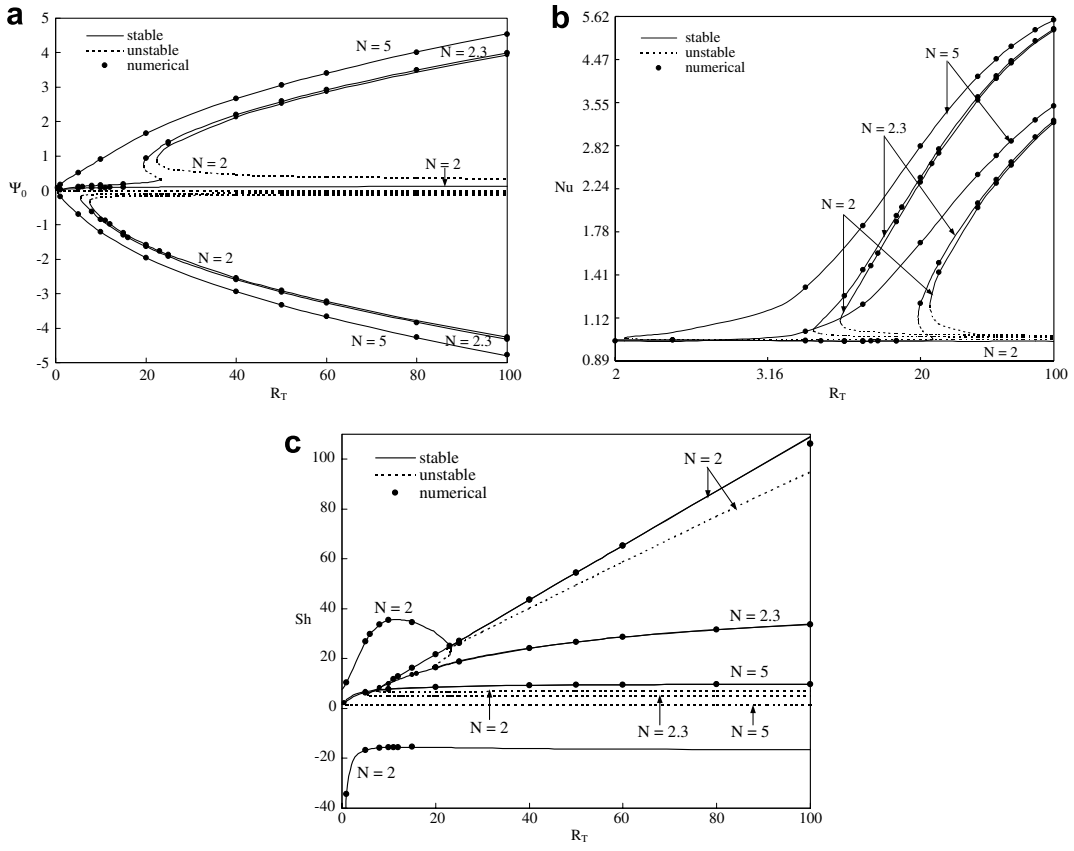

Fig. 4. Effect of N and R_T on: the flow intensity (a), the Nusselt number (b) and the Sherwood number (c) for $Le = 10$, $a = 0.2$ and $\varphi = 2$.

$N = 2.3$, the Sherwood number corresponding to the stable solutions exhibits different behaviors at relatively small R_T. Thus, in the range $0 < R_T < 23.29$, Sh induced by the trigonometric solution increases towards a maximum reached at $R_T \approx 12$ and decreases after that. However, Sh induced by the clockwise solution undergoes an increase with R_T and the curves corresponding to both stable solutions lead almost to the same Sh when R_T exceeds 23.29. For $N = 2$, the Sherwood number corresponding to the trigonometric flow starting from $R_T = 0$, is negative, exhibits an asymptotic behavior at large R_T and tends towards infinity when R_T approaches zero. In fact, as R_T tends towards 0, Sh tends towards the value of the purely diffusive regime given by Eq. (22) which is infinite in this case since $\varphi = N$. Note also that this situation is characterized by a zero concentration difference between top and bottom walls of the porous layer. Such a phenomenon is not possible in the absence of the Soret effect. Negative values of Sh indicate that there is an accumulation of solute on the upper boundary; situation becoming possible only when $M > 0$ and the magnitude of the thermodiffusion solute flux is large enough to compensate the external solute flux j' which salts the porous layer from below. The two other stable solutions induce nearly the same Sh which increases almost linearly with R_T. Analytically, it is demonstrated that for the particular case where $\varphi = N$, Sh exhibits a linear variation at large R_T for the solutions characterized by a Ψ_0 varying as $R_T^{1/2}$. This variation is such that $Sh \approx Le(\varphi + Le)[10(Le + 1)]^{-1} R_T$, and it applies to the regions III and IV. It is clear that this Sherwood number becomes independent of the lateral heating at large R_T. In addition, the unstable branches present different behaviors as shown in Fig. 4c. Note finally that, generally, for the situations corresponding to $N \neq \varphi$, Sh exhibits an asymptotic evolution with R_T for all the solutions.

4.3. Effect of the thermodiffusion on the multiplicity of solutions

The effect of the Soret parameter, φ, on the flow intensity, the Nusselt Number and the Sherwood Number, corresponding to the different solutions is illustrated in Fig. 5a–c for $Le = 3$, $R_T = 100$, $N = 2$ and $a = 0$ and 0.1. Fig. 5a shows that, for $a = 0$, three solutions are possible for $\varphi < 1.72$: two convective solutions and the rest sate which is found unstable below this critical value of φ. The curves of Ψ_0 corresponding to trigonometric and clockwise flows are symmetrical with respect to the horizontal axis $\Psi_0 = 0$. For a given value of φ, these solutions have the same intensities and generate the same Nusselt and Sherwood numbers. When φ exceeds 1.72, two other but unstable solutions appear. The flow intensities of the stable/(unstable) solutions decrease/(increase) with φ and only the rest state solution persists for $\varphi > 12.74$. In the

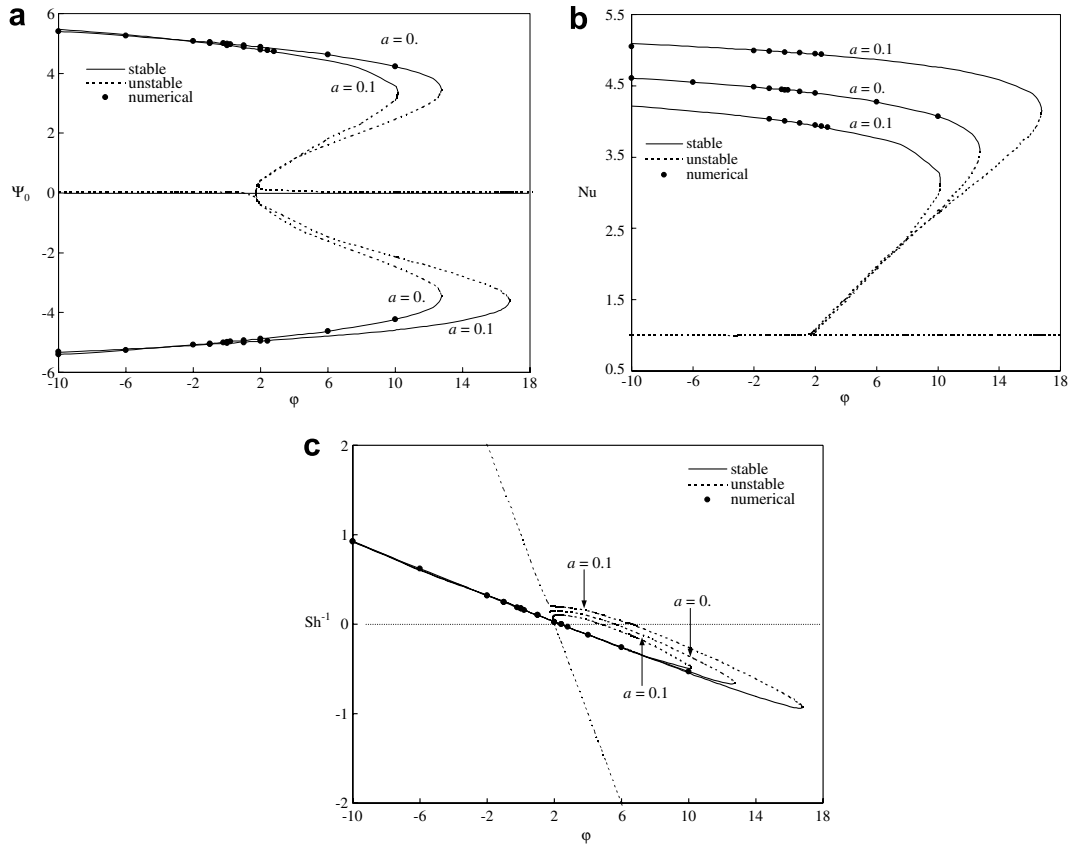

Fig. 5. Effect of φ on: the flow intensity (a), the Nusselt number (b) and the Sherwood number (c) for $R_T = 100$, $Le = 3$, $N = 2$ and $a = 0$ and 0.1.

presence of the perturbating lateral heating, illustrated here for $a = 0.1$, the symmetry observed for $a = 0$ is destroyed. For this case, three convective solutions are obtained for relatively small values of φ. Two among these solutions induce trigonometric flows; one is stable and the other is unstable and very close to the rest state. The third solution induces a clockwise stable flow. The increase of φ induces a slight decrease of Ψ_0 corresponding to the stable solutions while the intensity of the unstable trigonometric flow decreases slightly with φ in the vicinity of the rest state until the change of its sign which occurs at $\varphi = 1$. Above the latter critical value, the unstable flow becomes clockwise and its intensity increases quickly with φ. Two other unstable trigonometric solutions appear from $\varphi = 1.9$ such that the number of the convective solutions becomes five in a given range of φ. When φ exceeds 10.16, two among the previous solutions disappear and only one trigonometric solution persists for $\varphi > 16.78$ (the latter is very close to the rest state). It can be concluded that the increase of φ, above some threshold, reduces the number of solutions to one. Note that this analytical solution is verified numerically in the case of $a = 0$ but, in the case of $a = 0.1$, the numerical code leads to an oscillatory regime, it converges to the analytical solution only if R_T is small enough.

The evolution of Nu with φ is presented in Fig. 5b for the different solutions. Generally, it is seen that the heat transfer induced by the stable branches decreases with φ but remains always higher than that corresponding to the unstable branches. Note also that the heat transfer may be considerably affected by the Soret effect. For example, in the case of $a = 0$, the convective solutions disappear leading to an important reduction of Nu when φ exceeds 12.74. When the attention is focused on the stable solutions, Fig. 5b indicates that Nu increases with a in the case of clockwise flows but the tendency is inverted in the case of trigonometric flows.

The thermodiffusion effect on the mass transfer is illustrated in Fig. 5c in terms of the inverse of Sherwood number, Sh^{-1}, versus φ. The use of Sh^{-1}, avoids the singularities in the curves when the concentration difference between top and bottom walls of the enclosure becomes zero. It is seen that the stable solutions generate nearly the same transfer of mass for both values of a. By increasing φ, these solutions lead to a decrease of Sh^{-1} which changes the sign at $\varphi = 2.3$; value above which the concentration becomes more important on the top wall compared to that on the bottom wall. The unstable branches induce different mass transfers and generate also a change in the sign of Sh.

4.4. Effect of the lateral heating on the multiplicity of solutions

The effect of the lateral heating on the different convective solutions, obtained for $R_T = 100$, $Le = 5$, $N = -1.2$ and $\varphi = -0.6$ is presented in Figs. 6a–c. According to

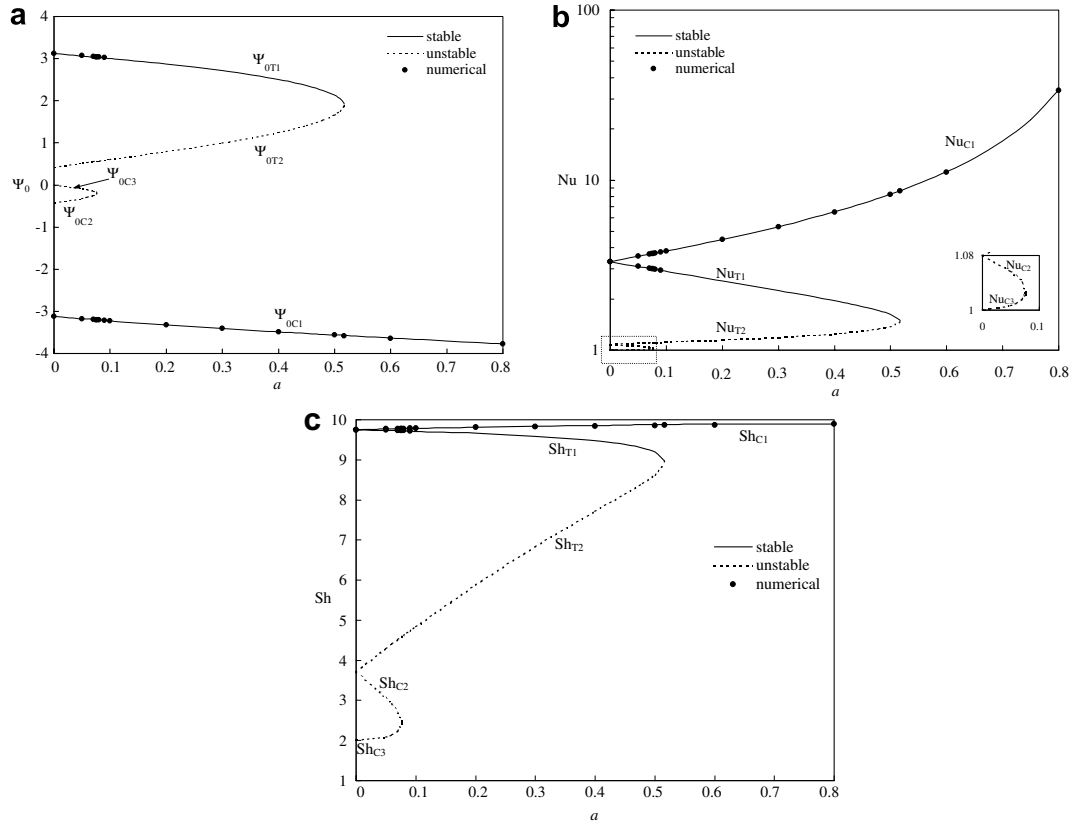

Fig. 6. Effect of a on: the flow intensity (a), the Nusselt number (b) and the Sherwood number (c) for $R_T = 100$, $Le = 5$, $N = -1.2$ and $\varphi = -0.6$.

Fig. 6a, five convective solutions are possible at relatively small values of a. Three among these solutions are clockwise with the intensities Ψ_{0C1}, Ψ_{0C2} and Ψ_{0C3} as indicated in Fig. 6a while the two others are trigonometric with the intensities Ψ_{0T1} and Ψ_{0T2}. For $a = 0$ (i.e. in the absence of lateral heating), $\Psi_{0C1} = -\Psi_{0T1}$, $\Psi_{0C2} = -\Psi_{0T2}$ and $\Psi_{0C3} = 0$ (rest state). The increase of a leads to a reduction of $|\Psi_{0C2}|$ and an increase of $|\Psi_{0C3}|$ until reaching a critical value of a ($a_{cr} \approx 0.0762$) where these intensities become equal and the two corresponding solutions disappear above this threshold. A similar behavior is observed for the solutions characterized by the intensities Ψ_{0T1} and Ψ_{0T2}. However, the disappearance of these solutions is delayed until $a_{cr} \approx 0.5167$; the threshold above which only one clockwise solution subsists. Hence, the intensification of the lateral heating leads to the disappearance of the multiplicity of solutions.

Fig. 6b illustrates the variations of Nu with a for the different solutions obtained. The branches Nu_{C1}, Nu_{C2}, Nu_{C3}, Nu_{T1} and Nu_{T2} correspond respectively to the solutions with the intensities Ψ_{0C1}, Ψ_{0C2}, Ψ_{0C3}, Ψ_{0T1} and Ψ_{0T2}. In the absence of the lateral heating ($a = 0$), $Nu_{C1} = Nu_{T1}$, $Nu_{C2} = Nu_{T2}$ and $Nu_{C3} = 1$. By increasing a, Nu_{T1} (Nu_{C3}) decreases while Nu_{T2} (Nu_{C2}) increases towards the same value reached at $a_{cr} \approx 0.5167$ ($a_{cr} \approx 0.0762$). The stable clockwise solution, the one maintained over all the range of a, is the most favourable to the heat transfer. The variations of Sh with a (Fig. 6c) are globally similar to those exhibited by Nu. However, in the case of the stable clockwise solution, the increase of Sh with a is very slow compared to the increase of Nu.

5. Conclusion

Double diffusive convection induced in a horizontal porous layer subject to uniform fluxes of heat and mass is studied analytically and numerically in the presence of Soret effect. The obtained results show that the φ–N plane can be divided into four regions with different characteristics in terms of multiplicity of solutions. It is found that there is a region where only one solution is obtained and another region where up to five analytical solutions are possible (three of them were validated numerically). It is also found that the increase of the Soret parameter φ above some threshold leads to the disappearance of the multiplicity of solutions. Although the external mass flux is imposed from below, there are situations where the Sherwood number becomes negative which means that thermodiffusion may create an accumulation of solute on the upper boundary. The evolution of Nusselt number with R_T is always characterized by an asymptotic behavior while that of Sh is found to be more complex in general. Finally, it is observed that the Soret effect may modify considerably the heat transfer. For example, it can lead to a complete disappearance of the flow and hence brings back the system to a purely conductive state.

References

Alex, S.M., Patil, P.R., 2001. Effect of variable gravity field on Soret driven thermosolutal convection in a porous medium. Int. Commun. Heat Mass Transfer 28, 509–518.

Bahloul, A., Boutana, N., Vasseur, P., 2003. Double-diffusive and Soret-induced convection in a shallow horizontal porous layer. J. Fluid Mech. 491, 325–352.

Benano-Melly, L.B., Caltagirone, J.P., Faissat, B., Montel, F., Costeseque, P., 2001. Modeling Soret coefficient measurement experiments in porous media considering thermal and solutal convection. Int. J. Heat Mass Transfer 44, 1285–1297.

Bennacer, R., Mahidjiba, A., Vasseur, P., Beji, H., Duval, R., 2003. The Soret effect on convection in a horizontal porous domain under cross temperature and concentration gradients. Int. J. Numer. Methods Heat Fluid Flow 13, 199–215.

Bourich, M., Hasnaoui, M., Amahmid, A., Mamou, M., 2005. Onset of convection and finite amplitude flow due to Soret effect within a horizontal sparsely packed porous enclosure heated from below. Int. J. Heat Fluid Flow 26, 513–525.

Bourich, M., Hasnaoui, M., Amahmid, A., Mamou, M., 2004a. Soret convection in a shallow porous cavity submitted to uniform fluxes of heat and mass. Int. Commun. Heat Mass Transfer 31, 773–782.

Bourich, M., Amahmid, A., Hasnaoui, M., 2004b. Double diffusive convection in a porous enclosure submitted to cross gradients of temperature and concentration. Energy Convers. Manage. 45, 1655–1670.

Er-Raki, M., Hasnaoui, M., Amahmid, A., Mamou, M., 2006. Soret effect on the boundary layer flow regime in a vertical porous enclosure subject to horizontal heat and mass fluxes. Int. J. Heat Mass Transfer 49, 3111–3120.

Joly, F., Vasseur, P., Labrosse, G., 2001. Soret instability in a vertical Brinkman porous enclosure. Numer. Heat Transfer, Part A 39, 339–359.

Karcher, C., Müller, U., 1994. Bénard convection in binary mixture with a nonlinear density–temperature relation. Phys. Rev. E 49, 4031–4043.

Mansour, A., Amahmid, A., Hasnaoui, M., Bourich, M., 2006. Numerical study of the multiplicity of solutions induced by thermosolutal convection in a square porous cavity heated from below and submitted to horizontal concentration gradient in the presence of Soret effect. Numer. Heat Transfer, Part A 49, 69–94.

Marcoux, M., Charrier-Mojtabi, M.C., Bergeon, A., 1998. Naissance de la thermogravitation dans un mélange binaire imprégnant un milieu poreux. Entropie 214, 31–36.

Platten, J.K., Costesèque, P., 2004. The Soret coefficient in porous media. J. Porous Media 7 (4), 317–329.

Rehberg, I., Ahlers, G., 1985. Experimental observation of a codimension-two bifurcation in a binary fluid mixture. Phys. Rev. Lett. 55, 500–503.

Rosanne, R., Paszkuta, M., Tevissen, E., Adler, P.M., 2003. Thermodiffusion in a compact clay. J. Colloid Interface Sci. 267, 194–203.

Ryskin, A., Müller, H.W., Pleiner, H., 2003. Thermal convection in binary fluid mixtures with a weak concentration diffusivity, but strong solutal buoyancy forces. Phys. Rev. E 67, 1–8.

Sovran, O., Charrier-Mojtabi, M.C., Mojtabi, A., 2001. Naissance de la convection thermo-solutale en couche poreuse infinie avec effet Soret, vol. 329. Comptes-Rendus de l'Académie Sciences, Paris, pp. 287–293.

Trevisan, O.V., Bejan, A., 1986. Mass and heat transfer by natural convection in a vertical slot filed with porous medium. Int. J. Heat Mass Transfer 29, 403–415.